

MAGNETIC INHIBITION OF ACCRETION AND OBSERVABILITY OF ISOLATED OLD NEUTRON STARS

O. D. TOROPINA

Space Research Institute, Russian Academy of Sciences, 84/32 Profsoyuznaya, Moscow 117997, Russia;
toropina@iki.rssi.ru

M. M. ROMANOVA

Department of Astronomy, Cornell University, Ithaca, NY 14853-6801; romanova@astro.cornell.edu

YU. M. TOROPIN

CQG International Limited, 10/5 Sadovaya-Karetnaya, Building 1, Moscow 103006, Russia;
ytoropin@cqg.com

AND

R. V. E. LOVELACE

Department of Astronomy, Cornell University, Ithaca, NY 14853-6801; rv11@cornell.edu

Received 2003 February 22; accepted 2003 April 19

ABSTRACT

Isolated old neutron stars moving through the interstellar medium capture matter gravitationally. If the star is unmagnetized, the captured matter accretes to the surface of the star. However, the stars are expected to be magnetized. Moreover, some of the stars may be in the “propeller” stage of evolution. Both the magnetic field and the rotation act to decrease the accretion rate to the surface of the star. Here we consider stars that are past the propeller stage, so that rotation is unimportant. The influence of the magnetic field on the accretion rate to the star’s surface is investigated using axisymmetric, resistive magnetohydrodynamic (MHD) simulations. Matter is taken to inflow at the Bondi rate for a nonmagnetized star, and we verify that stationary Bondi accretion flows occur in the absence of a magnetic field. For a magnetized star we find that an outward-propagating shock wave forms and that a new stationary, subsonic accretion flow is set up inside this shock, as first pointed out by Toropin et al. in 1999. Accretion to the surface of the star \dot{M} occurs along two columns aligned with the magnetic axis of the star. Only a fraction of the Bondi flux \dot{M}_B accretes to the surface of the star. The empirical dependences we find are $\dot{M}/\dot{M}_B \propto (R_*/R_A)^5$ for $R_A/R_* \sim 6$ –10, where R_A is the Alfvén radius. In terms of the star’s magnetic moment μ , we find $\dot{M}/\dot{M}_B \propto \mu^{-3}$. The accretion rate decreases as the magnetic diffusivity of the plasma η_m decreases, $\dot{M} \propto (\eta_m)^{0.6}$. We conclude that even a very small residual magnetic field, $B \sim 10^6$ – 10^8 G, may significantly reduce the accretion rate to the surface of the star and thereby make the accretion luminosity undetectable. The possibility of enhanced accretion owing to three-dimensional instabilities remains to be investigated. The results presented here may also be applicable to wind-fed X-ray stars in binary systems.

Subject headings: accretion, accretion disks — magnetic fields — plasmas — stars: magnetic fields — stars: neutron — X-rays: stars

1. INTRODUCTION

Most neutron stars are thought to be isolated old neutron stars (IONSs), which are invisible. The estimated number of IONSs in our Galaxy is 10^8 – 10^9 (see, e.g., Arnett, Schramm, & Truran 1989; Narayan & Ostriker 1990). The closest IONSs are expected to be observable owing to accretion of matter from the interstellar medium (ISM) to their surfaces. These objects have low luminosities, $L \sim 10^{28}$ – 10^{31} ergs s^{-1} , but are numerous, $\sim 10^2$ – 10^3 (Ostriker, Rees, & Silk 1970; Schvartsman 1971; Treves & Colpi 1991; Blaes & Madau 1993; Treves et al. 2000; Popov et al. 2000). However, only a few IONS candidates were found in careful searches (see, e.g., review by Treves et al. 2000). A number of factors can influence the observability of IONSs.

1.1. Inhibition of Accretion Due to High Velocities

Recent analyses of the distribution of velocities of pulsars (e.g., Cordes & Chernoff 1998; Popov et al. 2000) have shown that their average velocities v are higher ($v \approx 180$ km s^{-1} ; Cordes & Chernoff 1998) than those taken in early esti-

mations ($v \approx 10$ km s^{-1}), so that the gravitational radius $R_{\text{acc}} = 2GM/v^2 \propto 1/v^2$ and the accretion rate $\dot{M} = \pi R_{\text{acc}}^2 \rho v \propto 1/v^3$ are smaller (Bondi & Hoyle 1944; Bondi 1952). Here M is the mass of the star and ρ is the density of the ISM. The dependence of the accretion rate on the velocity is very strong, and this may be one of the reasons why only a few IONS candidates have been observed. However, a significant number of neutron stars still may have comparatively small velocities, $v < 50$ – 100 km s^{-1} . Thus, the effect of a large average velocity does not eliminate the possibility of observable nearby IONSs.

1.2. Decrease of the Accretion Rate Due to Preheating of the Ambient Gas

The accretion rate onto isolated neutron stars may decrease because of preheating of the infalling gas. The temperature of the infalling gas may increase as a result of its interaction with the radiation field of the star (Ostriker et al. 1976; Madau & Blaes 1994; Blaes, Warren, & Madau 1995).

On the other hand, the heating may be connected with compression of the weak ambient magnetic field and subse-

quent reconnection (Bisnovatyi-Kogan & Lovelace 1997, 2000; Igumenshchev & Narayan 2002). This interesting mechanism of heating should be further investigated in analytical and numerical study.

1.3. Inhibition of Accretion at the “Propeller” Stage

Accretion to the surfaces of isolated neutron stars in the propeller stage of evolution may be strongly suppressed because of the centrifugal force of the star’s rotating field (Illarionov & Sunyaev 1975; Davies, Fabian, & Pringle 1979; Davies & Pringle 1981; Wang & Robertson 1985; Lipunov 1992; Ikhsanov 2002; Romanova et al. 2003). If the accreting matter has significant angular momentum, then an accretion disk is expected to form around the magnetized star (Beloborodov & Illarionov 2001). In this case, the propeller effect may also act to prevent incoming matter from reaching the star’s surface (Lovelace, Romanova, & Bisnovatyi-Kogan 1999). Livio, Xu, & Frank (1998) and Colpi et al. (1998) recognized that IONSS may be in the propeller stage during a cosmological time and argue that this may be the main reason for the small number of IONSS. The duration of the propeller stage depends on the rate of the star’s field decay. It is believed that the magnetic field of the star, $B_0 \sim 10^{12}$ G, decays rapidly during a characteristic time, $\tau \sim 10^7\text{--}10^9$ yr, to much smaller values, $B_m \sim 10^9\text{--}10^{10}$ G. Subsequently, this small field decays with a much longer timescale, which may be of the order of the cosmological time T_{cos} (see, e.g., Urpin & Muslimov 1992; Phinney & Kulkarni 1994; Urpin & Konenkov 1997). Livio et al. (1998) have shown that if the initial magnetic field does not decay rapidly and if the final field is not very small, $B_m \gtrsim 5 \times 10^9$, then IONSS will be in the propeller stage during a cosmological time. However, for a range of other parameters, they found that the duration of the propeller stage is shorter than T_{cos} . These objects are expected to accrete matter.

1.4. Magnetic Inhibition of Accretion

Subsequent to the propeller stage, matter tends to accumulate around the star. It was recognized in the 1970s that the magnetic fields of highly magnetized stars may strongly suppress accretion in the absence of instabilities that transport matter across the magnetic field. It was argued that some matter may penetrate through the magnetosphere either through the equatorial regions owing to the Rayleigh-Taylor instability (Arons & Lea 1976a, 1976b; Elsner & Lamb 1977), through direct accretion from the polar regions (see, e.g., Michel 1977a, 1977b, 1977c), or as a result of Bohm diffusion across the magnetic field (Ikhsanov & Pustil’nik 1996; Ikhsanov 2002). There is still no accepted model for the fraction of the incoming matter that accretes to the surface of a star and the mechanism(s) mainly responsible. This problem is inescapably multidimensional, so multidimensional MHD simulations can be valuable for understanding the accretion to magnetized stars.

Toropin et al. (1999, hereafter T99) performed the first numerical two-dimensional (axisymmetric) MHD simulations of the spherical accretion to a star with a *dipole* magnetic field. The Bondi (1952) solution was used as initial and external boundary conditions for the accreting matter. Interesting and unexpected features were observed in the simulations. A shock wave formed around the magneto-

sphere and propagated outward. A new regime of subsonic, low-velocity accretion formed inside the shock wave. The accretion rate to the star was significantly smaller than the Bondi rate, $\dot{M} < \dot{M}_B$. No stationary shock wave was observed at the magnetopause. These simulations have shown that the dipole magnetic field decreases the accretion rate to the surface of the star.

Recently, Igumenshchev & Narayan (2002) performed three-dimensional MHD simulations of spherical accretion to a gravitating center (black hole) in presence of the *ordered* large-scale magnetic field threading the disk. They also used the Bondi flow for setup of the initial and boundary conditions, as T99 did. They have shown that the compression of the ordered magnetic field, with subsequent reconnection and heating, leads to inhibition of accretion to the gravitating center and to formation of two accreting regions separated by the shock wave, as in T99. This magnetic/heating mechanism of inhibition of accretion may also be important for observability of IONSS. However, in this paper we suppose that accreting matter is not magnetized, and we investigate the influence of the internal dipole magnetic field of the star on the accretion rate.

In our first paper (T99), only weak dipole magnetic fields were investigated, with the Alfvén radii $R_A/R_* < 3$. Even such a weak magnetic field suppressed the accretion rate to the surface of the star: $\dot{M}/\dot{M}_B \sim 0.5\text{--}0.8$. In reality, the Alfvén radius may be much larger than the radius of the star. In this paper, we report simulations for much larger values of R_A , $R_A/R_* \sim 6\text{--}10$, and for an improved, more realistic model of the star.

In § 2, we describe the numerical model. In § 3, we discuss the main results of the numerical simulations. In § 4, we show an example of magnetic inhibition of accretion by a magnetized star. In § 5, we give the conclusions from this work.

2. NUMERICAL MODEL

The plasma accretion to a magnetized star is simulated with a resistive hybrid MHD code based on the method of local iterations and the flux-corrected transport method (Zhukov, Zabrodin, & Feodoritova 1993). The code was used in our earlier simulations of Bondi accretion to a magnetized star (T99), propagation of a magnetized star through the ISM (Toropina et al. 2001), and spherical accretion to a star in the propeller regime (Romanova et al. 2003). The equations for resistive MHD are

$$\frac{\partial \rho}{\partial t} + \nabla \cdot (\rho \mathbf{v}) = 0, \quad (1)$$

$$\rho \frac{\partial \mathbf{v}}{\partial t} + \rho (\mathbf{v} \cdot \nabla) \mathbf{v} = -\nabla p + \frac{1}{c} \mathbf{J} \times \mathbf{B} + \mathbf{F}^g, \quad (2)$$

$$\frac{\partial \mathbf{B}}{\partial t} = \nabla \times (\mathbf{v} \times \mathbf{B}) + \frac{c^2}{4\pi\sigma} \nabla^2 \mathbf{B}, \quad (3)$$

$$\frac{\partial (\rho \varepsilon)}{\partial t} + \nabla \cdot (\rho \varepsilon \mathbf{v}) = -p \nabla \cdot \mathbf{v} + \frac{\mathbf{J}^2}{\sigma}. \quad (4)$$

The equation of state is that for an ideal gas, $p = (\gamma - 1)\rho\varepsilon$, with specific heat ratio $\gamma = 7/5$. The equations incorporate Ohm’s law, $\mathbf{J} = \sigma(\mathbf{E} + \mathbf{v} \times \mathbf{B}/c)$, where σ is the electrical conductivity. The associated magnetic diffusivity,

$\eta_m \equiv c^2/(4\pi\sigma)$, is considered to be a constant within the computational region. In equation (2) the gravitational force, $\mathbf{F}^g = -GM\rho\mathbf{R}/R^3$, is due to the central star.

We use a cylindrical, inertial coordinate system (r, ϕ, z) and assume axisymmetry ($\partial/\partial\phi = 0$). The vector potential \mathbf{A} is calculated so that $\nabla \cdot \mathbf{B} = 0$ at all times. The full set of equations is given in T99.

2.1. Simulation Region and Grid

Simulations were done in a cylindrical region ($0 \leq z \leq Z_{\max}$, $0 \leq r \leq R_{\max}$; see Fig. 1). The size of the region was taken to be $R_{\max} = Z_{\max} = 0.141R_B$, where $R_B \equiv GM/c_\infty^2$ is the Bondi radius, with c_∞ the sound speed in the undisturbed medium at infinity. The size of the region is smaller than the sonic radius of the Bondi flow, $R_s = [(5 - 3\gamma)/4]R_B$ ($=0.2R_B$ for $\gamma = 7/5$). Thus, matter inflows supersonically to the computational region. The inflow rate is taken to be the Bondi (1952) accretion rate,

$$\dot{M}_B = 4\pi\lambda(GM_*)^2\rho_\infty/c_\infty^3, \quad (5)$$

where $\lambda = 0.625$ for $\gamma = 7/5$. The incoming matter is unmagnetized. We use a uniform (r, z) grid with $N_R \times N_Z$ cells. For the results discussed here, $N_R \times N_Z = 513 \times 513$.

The “model star” is a cylinder of radius R_* and half-axial length Z_* , with $R_* = Z_* \ll R_{\max}$, Z_{\max} . For the results presented here, $R_* = Z_* = 0.0044R_B$, so that $R_{\max} = Z_{\max} = 32R_*$. The grid size, $DR = R_{\max}/N_R = 2.76 \times 10^{-4}R_B$, is about 16 times smaller than the star’s radius. This DR is one-half the value of that in T99.

2.2. Initial Conditions

Initially, the magnetic field of the star is a pure dipole field, $\mathbf{B} = [3\mathbf{R}(\boldsymbol{\mu} \cdot \mathbf{R}) - R^2\boldsymbol{\mu}]/R^5$, with $\boldsymbol{\mu} = \mu\hat{z}$ and vector potential $\mathbf{A} = \boldsymbol{\mu} \times \mathbf{R}/R^3$. All hydrodynamic quantities (ρ , v_r , v_z , and ε) are set equal to the values for the Bondi flow with $\gamma = 7/5$ (Bondi 1952). The matter is not rotating ($v_\phi = 0$), and the magnetic field has $B_\phi = 0$.

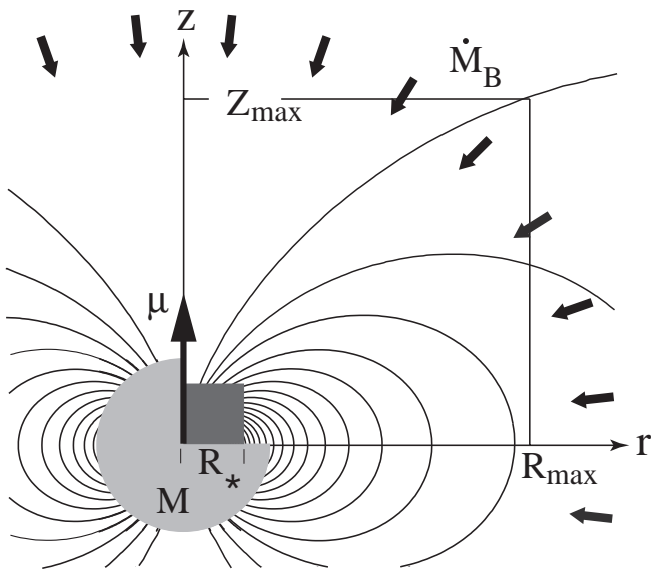


FIG. 1.—Geometry of the MHD simulation region, where \dot{M}_B is the Bondi accretion rate, μ is the magnetic moment of the star, R_* is the radius of the star, and (R_{\max}, Z_{\max}) are the limits of the computational region. In the described calculations, $R_* \ll R_{\max}$.

2.3. Boundary Conditions

At the outer boundaries ($r = R_{\max}$, $z = Z_{\max}$), the variables (ρ, \mathbf{v}) and ε were fixed equal to the Bondi values. The inflowing matter is assumed to be unmagnetized, so that $\mathbf{A} = 0$ and $B_\phi = 0$ at the outer boundaries. The incoming matter is not rotating, so that $v_\phi = 0$. The $z = 0$ plane is assumed to be a symmetry plane. The z -axis is the symmetry axis.

The model star in this paper is different from that in T99. In T99 we modeled the dipole magnetic field by a thin, current-carrying disk in the $z = 0$ surface. In present simulations, the model star represents a cylindrical box, with vector potential \mathbf{A} determined at the surface of this box. The value of the vector potential on this surface is fixed corresponding to the model star being a perfect conductor. Equivalently, the component of the \mathbf{B} field normal to the surface is fixed, but the other two components vary. The density and internal energy at the inner boundary (the model star) are set equal to small numerical values. For example, the density is set to be $\rho = 1$, while the density of the accreting matter is about 10^3 times larger. Incoming matter with higher values of these parameters is absorbed by the star (see also Ruffert 1994; T99). Velocities were set equal to zero at the inner boundary: $v_r = v_z = v_\phi = 0$. Test runs were performed with the “free” boundary conditions: $\partial v/\partial n = 0$. For a purely hydrodynamic spherical accretion flow, we verified that (for both conditions on the velocity) this accretor absorbs all incoming matter at the Bondi rate.

2.4. Dimensionless Units

We measure length in units of the Bondi radius R_B , density in units of the density at infinity ρ_∞ , and the magnetic field strength in units of B_0 , which is the field at the pole of the model star ($r = 0$, $z = Z_*$). We use the field strength parameter b_0 , defined as $\mathbf{A} = b_0\mathbf{A}_0$, to control the field strength of the star. We varied b_0 in the range 10–25. Pressure is measured in units of $B_0^2/8\pi$. The magnetic moment μ is measured in units of $\mu_0 = B_0R_B^3/2$. We measure velocity in units of the Alfvén speed $v_0 = B_0/(4\pi\rho_\infty)^{1/2}$. Time is measured in units of the “free-fall” time from a distance $r = R_{\max}$, $z = 0$; that is, $t_{\text{ff}} = R_{\max}^{3/2}/(2GM)^{1/2}$.

After putting the MHD equations in dimensionless form, one finds three dimensionless parameters, two of which are

$$\beta \equiv \frac{8\pi p_\infty}{B_0^2}, \quad \tilde{\eta}_m \equiv \frac{\eta_m}{R_B v_0}. \quad (6)$$

Here $\tilde{\eta}_m$ is the dimensionless magnetic diffusivity, and $p_\infty = \rho c_\infty^2/\gamma$ is the pressure at infinity. The third parameter, $GM/(R_B v_0^2) = \gamma\beta/2$, is of the order of β .

3. RESULTS OF SIMULATIONS

In simulations of accretion to an unmagnetized star, we observed that matter accretes supersonically at the Bondi rate (Bondi 1952). The velocity and density variations were those of the Bondi solution, and no discontinuities were observed in the simulation region. However, when the magnetic field of the star is included, the flow is very different from the hydrodynamical flow.

3.1. Matter Flow around the Magnetized Star

We observed that a shock wave forms around the magnetosphere of the star and propagates outward. A new subsonic accretion flow forms inside the shock wave, with velocity less than the Bondi value and density and temperature larger than the Bondi values (see also T99). The observed expanding shock wave represents a boundary between the new subsonic accretion flow with low accretion rate ($\dot{M} < \dot{M}_B$) around the magnetosphere and the initial supersonic Bondi flow.

Figure 2 shows a calculated flow at $t \approx 1.7t_{\text{ff}}$ for $\beta = 10^{-7}$, magnetic diffusivity $\tilde{\eta}_m = 10^{-5}$, and a field strength parameter $b_0 = 20$. Outside of the shock the flow is the spherically symmetric Bondi flow, while inside the shock the flow becomes anisotropic. Matter has a tendency to flow along the magnetic field lines starting from far distances. The thick solid line shows the Alfvén surface, where the matter energy density $\rho(\varepsilon + v^2/2)$ is equal to the magnetic energy density $B^2/8\pi$. The Alfvén surface is ellipsoidal, with an equatorial radius $R_A = 7.6R_*$ and an axial radius $R_A = 9.6R_*$. Inside the Alfvén surface matter tends to flow along the magnetic field lines.

Figure 3 shows the inner region of Figure 2. The plasma is seen to flow along the magnetic field lines to form polar accretion columns. The density in the accretion columns is 3–4 orders of magnitude larger than that in the equatorial plane. The dotted line corresponds to the Lundquist number, which is discussed in § 3.2.

Figure 4 shows the matter flux through spherical surfaces located at different radii R at a time $1.7t_{\text{ff}}$. The figure shows that the accretion rate is approximately constant out to the radius R_{sh} of the shock, which is propagating outward. This means that a new matter flow has been established around

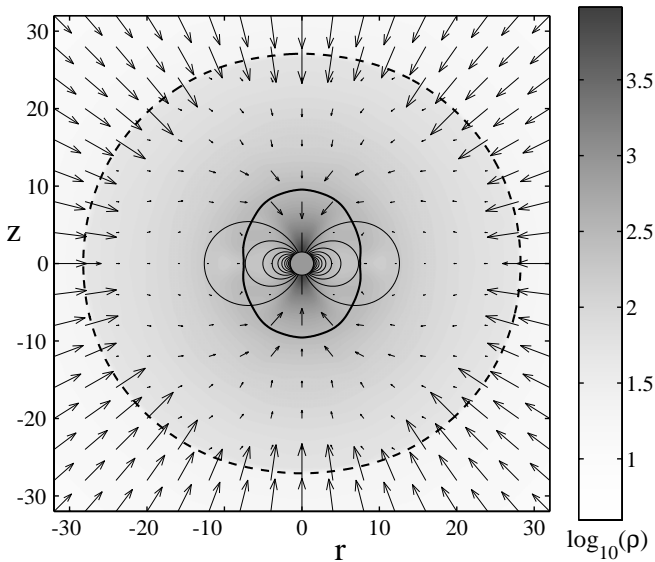


FIG. 2.—Example of the calculated accretion flow onto a star with a dipole magnetic field. The run is characterized by the dimensionless parameters $\beta = 10^{-7} \propto \dot{M}/\mu^2$, the parameter $b_0 = 20$, and dimensionless magnetic diffusivity $\tilde{\eta}_m = 10^{-5}$, where \dot{M} is the accretion rate and μ is the star's magnetic moment. The background gray scale represents the density of the flow and the solid lines the poloidal magnetic field lines. The length of the arrows is proportional to flow speed. The thick solid line shows the Alfvén surface. The dashed line shows the sonic surface. The flow becomes strongly anisotropic close to the dipole. The simulations were done on a grid with 513×513 cells. The accretion rate to the star is $\dot{M}/\dot{M}_B \approx 0.21$.

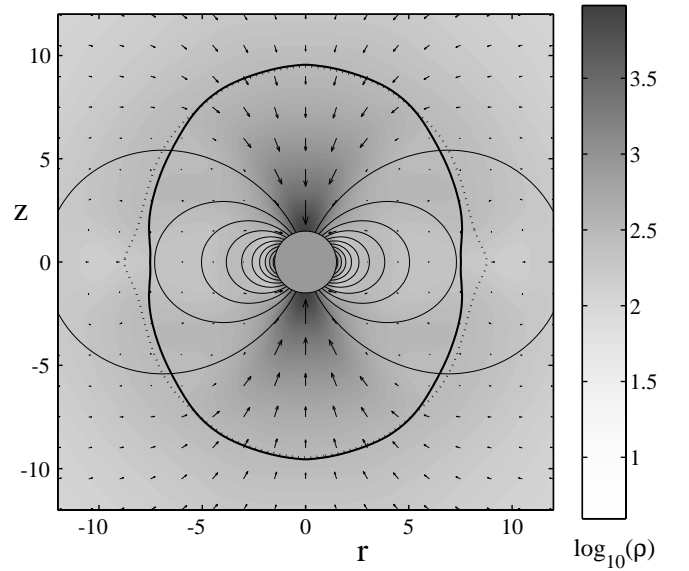


FIG. 3.—Enlarged view of the inner region of Fig. 2. The anisotropy of the flow is evident. The thick solid line shows the Alfvén surface. The dotted line shows the surface corresponding to Lundquist number $S = R_A v_A / \eta_m = 1$; inside this surface $S > 1$, while outside it $S < 1$.

the magnetized star and that it is *stationary*. At the shock wave $R = R_{\text{sh}}$, the accretion rate jumps up to the Bondi rate. Note that similar stationary inner subsonic regions were observed in our earlier simulations (T99). However, in T99 the size of the model star was 3 times larger. The accretion rate to the magnetized star equals to the accretion rate in this subsonic region, $\dot{M}/\dot{M}_B \approx 0.21$.

Figure 5 shows time evolution of the density ρ and velocity v at different fixed points of the stationary subsonic region. One can see that fluctuations of these parameters do not exceed 4%–5%. Thus, the local physical variables are time-independent after passage of the shock wave. Figures 4 and 5 demonstrate that the flow in the subsonic region is stationary in both space and time.

We stopped the simulations when the shock wave reached the outer boundaries of the simulation region. At this time

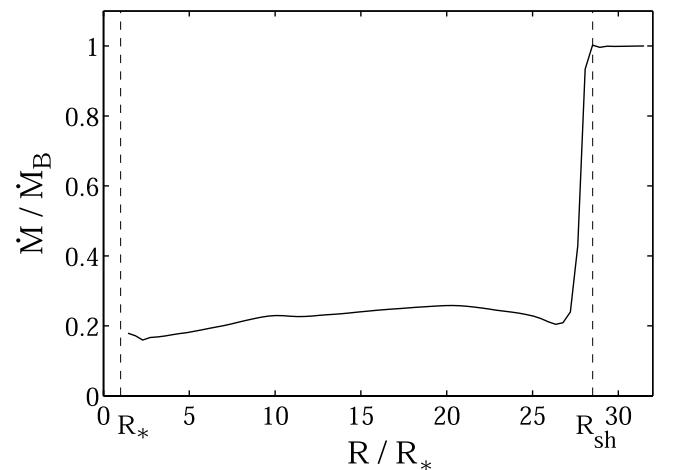


FIG. 4.—Mass accretion rate \dot{M} through the spheres of radii R at $t = 1.7t_{\text{ff}}$. R_* is the radius of the star and R_{sh} is the equatorial radius of the shock.

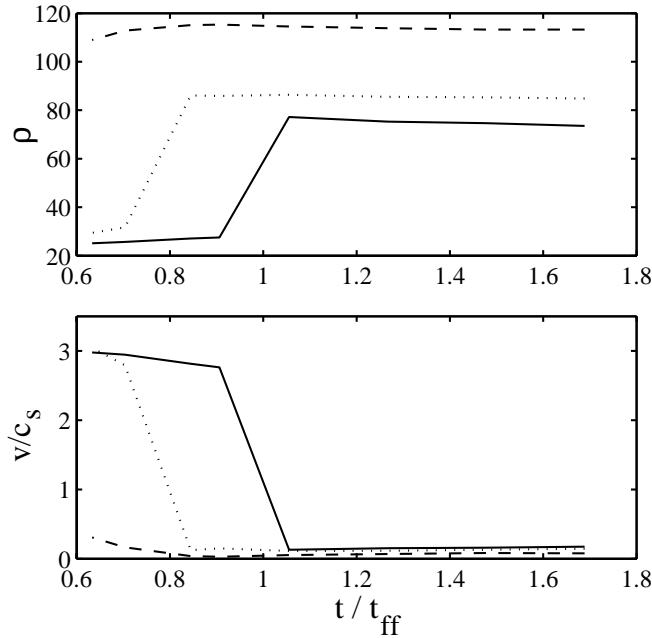


FIG. 5.—Evolution of density ρ and velocity v with time at different points: $R = 15R_*$ (dashed line), $18R_*$ (dotted line), and $20R_*$ (solid line). The local physical variables are time-independent after passage of the shock wave. Parameter fluctuations in this flow do not exceed 4%–5%.

the radius of the shock wave in the r -direction is several times larger than the Alfvén radius, $R_{\text{sh}}/R_A \approx 4.2$. This time corresponds to $t = 1.7t_{\text{ff}}$, where the t_{ff} is the free-fall time at $R = R_{\text{max}}$. It corresponds to $t \approx 15(t_{\text{ff}})_A$ dynamical timescales $(t_{\text{ff}})_A = R_A^{3/2}/(GM)^{1/2}$ measured at the Alfvén radius, $R = R_A \approx 7.6R_*$. This timescale is more appropriate for establishment of new stationary flow around the magnetosphere.

We performed a number of test simulations at smaller values of R_* and R_A and observed that in all runs the new stationary flow is reached rapidly at $t \approx (t_{\text{ff}})_A$. We subsequently observed that the stationary state was supported during many magnetospheric dynamical timescales, $t > 50\text{--}100(t_{\text{ff}})_A$. However, in this paper we focus attention on the larger magnetospheres.

Next, we investigate the dependence of the accretion rate on the magnetic moment of the star μ and on the magnetic diffusivity $\tilde{\eta}_m$.

3.2. Dependence of \dot{M} on the Star's Magnetic Moment

First, we fix the magnetic diffusivity $\tilde{\eta}_m = 10^{-5}$ and calculate the dependence of the accretion rate on the magnetic moment of the star μ . The radius of the star is fixed, so that we can change μ by changing the field strength parameter b_0 . Figure 6a shows the observed dependence, which is

$$\dot{M}/\dot{M}_B \propto \mu^{-3}. \quad (7)$$

Figure 6b shows the related dependence of \dot{M} on the Alfvén radius R_A ,

$$\dot{M}/\dot{M}_B \approx 6.5 \times 10^{-2} (10R_*/R_A)^5. \quad (8)$$

This dependence was derived for the limited range $R_A/R_* \approx 6\text{--}10$. In T99, where we had smaller values of

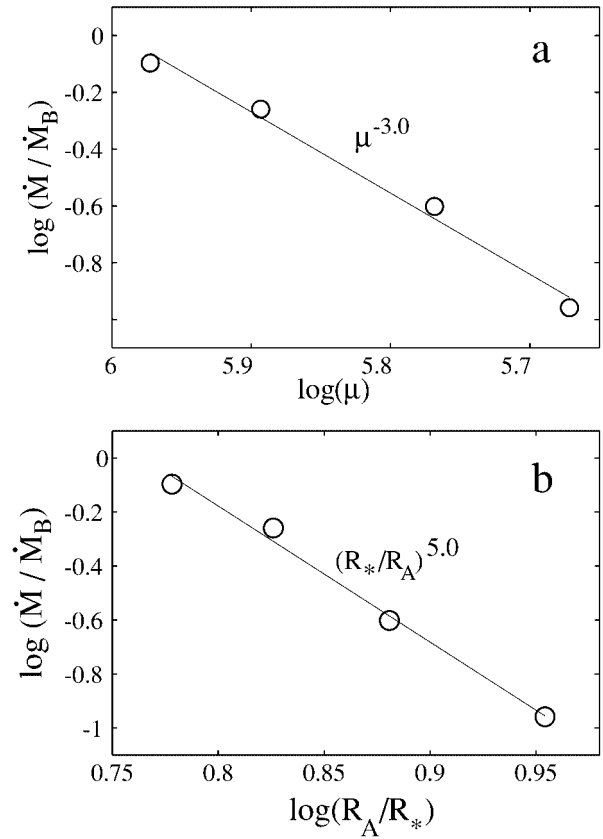


FIG. 6.—(a) Dependence of the accretion rate on the ratio of the Alfvén radius to the radius of the star R_A/R_* . (b) Dependence of the accretion rate on the magnetic moment μ .

$R_A/R_* \approx 2\text{--}3$, this dependence is slower, $\dot{M}/\dot{M}_B \sim (R_*/R_A)^{1.7}$. For $R_A \approx R_*$, $\dot{M} \approx \dot{M}_B$.

From Figure 3 one can see that matter tends to accrete strongly within cones aligned with the poles. As μ is increased the Alfvén surface moves away from the star, and the accretion columns have smaller opening angles. This dependence can be explained by the fact that at large μ the Alfvén radius is larger, so that the opening angle of the accretion columns is smaller. Figure 7 shows the differential matter accretion fluxes, $d\dot{M}/d\Omega$, through a sphere of radius $2R_*$ as a function of the colatitude θ for different magnetic moments μ . The accretion cones become narrower as μ increases.

3.3. Dependence of \dot{M} on Diffusivity

Next, we fix the value of the magnetic moment μ , fix $b_0 = 15$, and calculate the dependence of the accretion rate on the dimensionless magnetic diffusivity $\tilde{\eta}_m$ (eq. [6]). We find that the accretion rate decreases as $\tilde{\eta}_m$ decreases, as shown in Figure 8. Specifically,

$$\dot{M} \sim (\tilde{\eta}_m)^{0.6}, \quad (9)$$

for $\tilde{\eta}_m$ in the range 10^{-6} to $10^{-4.5}$. Plasma penetration across a magnetic field may be characterized by the magnetic Reynolds number, $\text{Re}_m = vR/\eta_m$, or by the Lundquist number, $S = v_A R/\eta_m$, where v is the local velocity of the flow, v_A is the local Alfvén velocity, and R is a characteristic scale, which we take to be R_A . If the velocity of the flow is high, then Re_m is larger and plasma penetration through magnetic

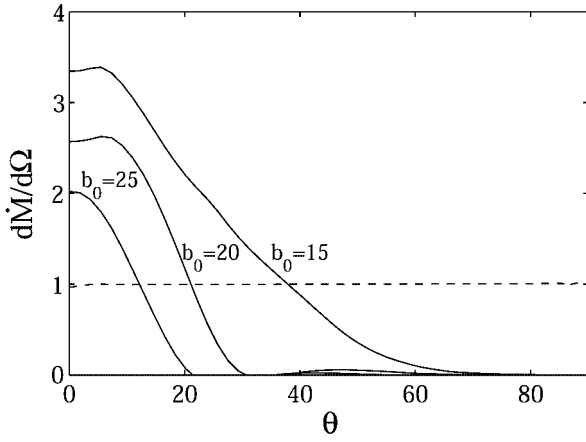


FIG. 7.—Differential mass accretion rate per unit solid angle $d\dot{M}/d\Omega$ as a function of the polar angle θ for different magnetic moments μ at a radius $2R_*$. The dashed line corresponds to Bondi accretion onto a non-magnetized star.

field lines is small, if $Re_m > 1$. However, in the case of accretion to a dipole, the velocities are high in the region of the poles, where matter moves along the magnetic field lines. In the equatorial region, the velocities are much smaller. For this reason, the Lundquist number seems to be more informative for analysis of plasma penetration through the magnetosphere. Namely, at small values of the magnetic field (far from the star), $S \ll 1$, and matter penetrates through magnetic field lines. Closer to the star, the magnetic field of the dipole increases, $S > 1$, and matter penetration across the magnetic field is reduced. Figure 3 shows the line $S = 1$, inside of which diffusion across the magnetic field is small.

For very small magnetic diffusivity, three-dimensional instabilities may be important in allowing the motion of plasma across the magnetic field (Arons & Lea 1976a, 1976b). Arons & Lea proposed that matter gravitationally accumulates around a magnetized star and then accretes through the magnetosphere owing to Rayleigh-Taylor instability. Axisymmetric simulations do not allow the required type of perturbation.

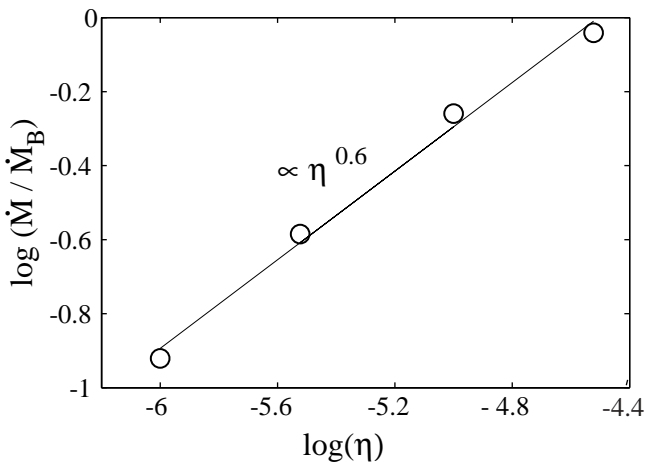


FIG. 8.—Dependence of the accretion rate \dot{M} on the dimensionless magnetic diffusivity $\tilde{\eta}_m$.

3.4. Evolution of the Flow at Large Distances

It is of interest to understand the evolution of matter flow at larger distances. We stopped the simulations when the shock wave reached the external boundary of the simulation region. We cannot expand the simulation region to much larger distances, because its size, $R_{\max} = Z_{\max} = 0.14R_B$, is already very close to the sonic surface of the Bondi flow $R_s = 0.2R_B$. A further increase of the region will lead to subsonic matter inflow to the region, which is problematic for the simulations. However, we can analyze the subsequent evolution of matter.

We chose the Bondi accretion flow as a convenient initial condition with a known distribution of physical parameters. We used the standard formula (eq. [5]) for Bondi accretion with $\lambda = 0.625$ (for $\gamma = 7/5$). This λ corresponds to the case in which the star absorbs *all* incoming matter. However, the magnetized star does not absorb all incoming matter; this is why the new type of matter flow is set up around the star with a lower accretion rate. This subsonic flow is also a Bondi flow, but at smaller λ . The region of lower accretion rate propagates outward. Initially, the shock wave separates these two regions. However, when the boundary between the two regions reaches the Bondi sonic radius R_s , it becomes subsonic and continues to propagate outward subsonically. The expansion will stop when the boundary reaches the Bondi radius, $R_B = GM/c_\infty^2$. At this point the information connected with the initial Bondi conditions will be gone. There will be no boundary between old and new flow. There will be only the flow with a smaller accretion rate, which starts at R_B and is stationary at all distances up to the star. Thus, the important part of the present simulations is the formation of a new stationary flow around the star. The shock wave is a temporary phenomenon. Such a shock may appear in nature, for example, in accretion to a star as it moves from a low- to a high-density region.

This type of accretion with a small accretion rate has an analogy with the formation of a hydrostatic atmosphere around a star that does not accrete. In such an atmosphere the matter flux is zero at all distances, and the atmosphere extends out to R_B . Such a solution, with $\lambda = 0$, was investigated by Bondi (1952) for $\gamma = 5/3$. In § 4.1, we discuss the Bondi solutions for the case of small λ .

The problem of establishment of a new accretion flow around semiabsorbing gravitating center was also investigated analytically by a number of authors (Sakashita 1974; Sakashita & Yokosawa 1974; Kazhdan & Lutskii 1977; Kazhdan & Murzina 1994). Kazhdan & Murzina (1994) analytically investigated the situation in which the accretion rate to the gravitating center is zero, or small, compared to the external accretion rate, while external matter accretes supersonically. They found a set of self-similar solutions that include an inner region with a low accretion rate, an outer region with a high accretion rate, and a shock wave that separates the two regions. They found that such an expanding shock wave is a common feature, if the central objects does not accrete all of the incoming matter. This analysis is consistent with our numerical simulations.

Inhibition of accretion by the magnetized star is different from the inhibition of accretion by preheating of the ambient matter studied, for example, by Blaes et al. (1995). In the case of preheating, the temperature of the surrounding gas is increased, which leads to an increase of the sound speed and to decrease of R_B and the accretion rate \dot{M}_B . In case of

accretion to a magnetized star, the heating is not significant, and the value of R_B does not change appreciably.

4. ACCRETION TO A NEUTRON STAR

Here we give the conversions of our dimensionless quantities to physical values. We consider accretion to a magnetized star with mass $M = 1.4 M_\odot = 2.8 \times 10^{33}$ g. The density of the ambient ISM is taken to be $\rho_\infty = 1.7 \times 10^{-24}$ g cm $^{-3}$ ($n_\infty = 1$ cm $^{-3}$). We consider a high sound speed in the ISM, $c_\infty = 100$ km s $^{-1}$, in order to have a smaller Bondi radius, compatible with our simulations. Such a large sound speed provides a rough way of modeling accretion to a neutron star moving supersonically. The characteristic radius for Bondi accretion is

$$R_B = GM_*/c_\infty^2 \approx 1.9 \times 10^{12} c_{100}^{-2} \text{ cm}, \quad (10)$$

and the accretion rate to a *nonmagnetized* star is

$$\dot{M}_B = 4\pi\lambda(GM_*)^2 \rho_\infty / c_\infty^3 \approx 4.6 \times 10^8 (n_1/c_{100}^3) \text{ g s}^{-1}, \quad (11)$$

where $\lambda = 0.625$ for $\gamma = 1.4$, $n_1 = n_\infty/1$ cm $^{-3}$, and $c_{100} = c_\infty/100$ km s $^{-1}$. In the absence of the magnetic field, matter will radiate near the stellar surface with a luminosity $L_{\text{BH}} \approx G\dot{M}_B M_*/R_* \approx 8.5 \times 10^{28}$ ergs s $^{-1}$, for a neutron star of radius $R_* = 10^6$ cm.

For a magnetized star, a simple model assumes that the matter with accretion rate \dot{M} infalls *supersonically*, with speed $v = (2GM/R)^{1/2}$, toward the star until the distance is reached where the ram pressure $\rho v^2 = \mathbf{B}^2/8\pi = \mu^2/(8\pi R^6)$ (see, e.g., Davidson & Ostriker 1973). This gives

$$R_A^{\text{sup}} = \left(\frac{\mu^2}{2\dot{M}\sqrt{2GM}} \right)^{2/7} \approx 6.8 \times 10^{10} \mu_{30}^{4/7} c_{100}^{6/7} n_1^{2/7} \text{ cm}, \quad (12)$$

where ‘‘sup’’ indicates supersonic flow and $\mu_{30} = \mu/10^{30}$ G cm 3 . Recall that the size of the model star is $R_* = 0.0044 R_B \approx 0.82 \times 10^{10}$ cm in all simulations.

4.1. Modified Bondi Accretion

For accretion to a magnetized, nonrotating star, the flow is in two conical regions aligned with the magnetic axis of the star. Thus, the treatment by Bondi (1952) is modified in the respect that mass conservation (instead of being $4\pi R^2 \rho v_r = \dot{M}$) is given approximately by

$$A(R)\rho v = \dot{M}, \quad (13)$$

where $A(R)$ is the area of the two conical flows and v is an average inflow velocity. From the Bernoulli equation,

$$\frac{v^2}{2} + \frac{c_s^2}{\gamma-1} - \frac{GM}{R} = \text{const}, \quad (14)$$

one obtains $f(u) = \lambda^{-q} g(x)$, where $f(u) = u^{4/(\gamma+1)} + u^{-q}/(\gamma-1)$, with $u = v/c_s$ the Mach number, and $c_s = (\gamma p/\rho)^{1/2}$ the sound speed, as given by Bondi (1952). Here $g(x) = [A(x)/4\pi R_B^2][1/x + 1/(\gamma-1)]$, with $x = R/R_B$, $R_B \equiv GM/c_\infty^2$, $q \equiv 2(\gamma-1)/(\gamma+1)$, and $\lambda \equiv \dot{M}/(4\pi\rho_\infty c_\infty R_B^2)$. In the spherical flow case for $\gamma < 5/3$, $g(x)$

has a minimum at a distance $\sim R_B$, which is the ‘‘throat’’ of the flow.

A rough approximation to the area of the accretion flow is $A = 4\pi R^3/(2R_A + R)$, where R_A is the Alfvén radius that separates the outer spherical flow from the inner conical flow. The inner conical flow is bounded by the dipole field of the star, so that the cylindrical radius is proportional to $R^{3/2}$. We estimate R_A below. For this dependence of A , one finds for $\gamma > 7/5$ that the minimum of $g(x)$ is at the surface of the star, so that the flow is subsonic (but possibly sonic at the star’s surface). For $\gamma < 7/5$, the minimum of $g(x)$ is at a finite distance, so that the flow goes from subsonic to supersonic. For $\gamma = 7/5$ the flow is subsonic if $R_A/R_B > 1/15$. The importance of the value $\gamma = 7/5$ in accretion flows in a dipole field was discussed in a different context by Koldoba et al. (2002).

Figure 9 shows that the observed flow $v_z(z)$ for $\gamma = 7/5$ is subsonic away from the star and sonic near the star’s surface. For this reason, we discuss the modified Bondi flows for the subsonic cases. The magnetic radius R_A is determined approximately by equating the gas pressure $\rho c_s^2/\gamma$ to the magnetic pressure $\mu^2/(8\pi R_A^6)$. For $\gamma = 7/5$ and $R_A/R_B < \gamma - 1$, this gives

$$R_A/R_B \approx [34.6\mu^2/(8\pi\rho_\infty c_\infty^2 R_B^6)]^{2/5} \approx 0.079 \mu_{30}^{4/5} c_{100}^4 n_1^{2/5}.$$

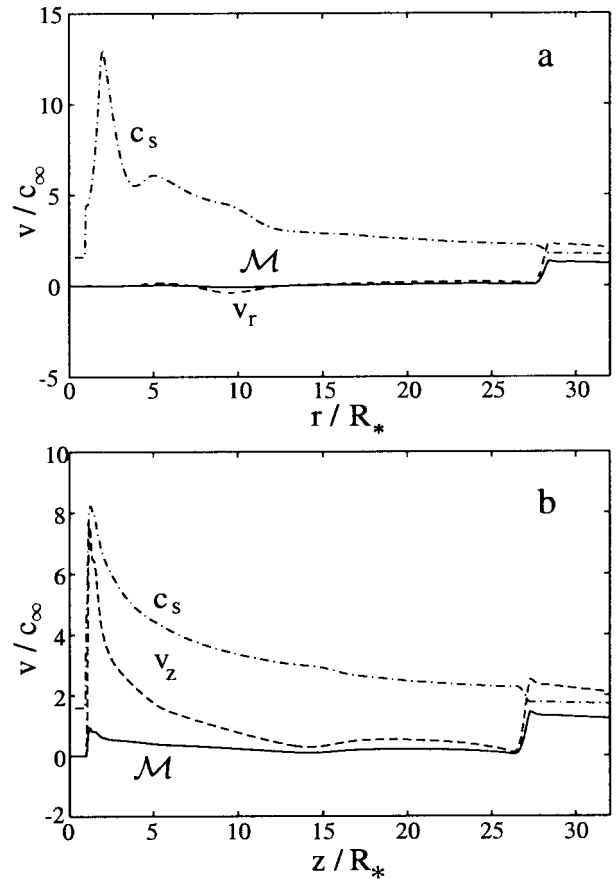


FIG. 9.—(a) Radial variation of the sound speed c_s (dot-dashed line), flow velocity $-v_r$ (dashed line), and Mach number $\mathcal{M} = -v_r/c_s$ (solid line) in the equatorial plane. (b) Axial velocity $-v_z$, sound speed, and Mach number along the z -axis. The case is the same as that shown in Figs. 2 and 3.

Equivalently,

$$R_A \approx 6.1 \times 10^{10} \mu_{30}^{4/5} c_{100}^2 / n_1^{2/5} \text{ cm} \quad (15)$$

for $\gamma = 7/5$. For $\gamma = 5/3$ and R_A/R_B unrestricted,

$$R_A/R_B = [4.6\mu^2 / (8\pi\rho_\infty c_\infty^2 R_B^6)]^{2/7} \approx 0.092\mu_{30}^{4/7} c_{100}^{20/7} / n_1^{2/7} .$$

Equivalently,

$$R_A \approx 9.1 \times 10^{10} \mu_{30}^{4/7} c_{100}^{6/7} / n_1^{2/7} \text{ cm} \quad (16)$$

for $\gamma = 5/3$.

The maximum steady accretion rate, corresponding to the maximum value of $\lambda (= \lambda_c)$, is determined by “choking” at the throat of the flow, where the minimum of $g (=g_m)$ occurs (Bondi 1952). This gives $\lambda_c = (g_m/f_m)^{1/q}$, where f_m is the minimum of $f(u)$, which is $f_m = (\gamma + 1)/[2(\gamma - 1)]$ at $u = 1$. For the cases in which the throat is at the surface of the star, $g_m = g(R_*)$. Thus, for $\gamma = 7/5$, $\lambda_c = R_B/(54R_A)$, which is at most somewhat less than unity ($\lambda_c \geq 0.278$) for the allowed range of R_A/R_B . In contrast, for $\gamma = 5/3$, $\lambda_c = R_*/(8R_A)$ may be very small compared with unity. In general, the steady accretion rate is $\lesssim (A\rho c_s)_{R_*}$ if the throat is at the surface of the star. From this one finds

$$\max(\dot{M}) \sim \frac{2\pi\kappa_\gamma R_*^{(5\gamma-7)/[2(\gamma-1)]}}{R_A K^{1/(\gamma-1)}} , \quad (17)$$

where $K = p/\rho^\gamma$ is the entropy and $\kappa_\gamma \equiv (\gamma - 1)^{1/q} / \gamma^{1/(\gamma-1)}$. An increase of the entropy near the star due to ohmic heating acts to reduce $\max \dot{M}$.

4.2. Application of Empirical Dependencies

From equations (7) and (8) we find that $R_A \propto \mu^{3/5}$, which is similar to the dependence of equation (15). The accretion rate to the surface of the star can be presented as a function of the ratio R_A/R_* . In the present simulations, we obtained the dependence for $R_A/R_* \approx 6-10$ as given by equation (8). The fact that \dot{M} decreases more strongly as R_A increases than indicated by equation (17) may be explained by the increase of the entropy $K = p/\rho^\gamma$ close to the star as R_A increases. In T99, where smaller values of R_A/R_* were investigated, the derived dependence is even less steep, $\dot{M}/\dot{M}_B \propto (R_*/R_A)^{1.7}$.

IONSs accrete matter from the ISM at very low accretion rates (see, e.g., eq. [11]) and for this reason have large magnetospheres. In these objects the accretion may be magnetically suppressed even for relatively weak magnetic fields. From equation (15), for $B_* = 10^{12}$ G we obtain $R_A/R_* \approx 6 \times 10^4$. For $B_* = 10^9$, we have $R_A/R_* \approx 240$. Values of $R_A/R_* \sim 10$, as in our simulations, correspond to $B_* \sim 10^6$ G. Thus, our simulation results indicate a strong inhibition of accretion to even very weakly magnetized neutron stars. The inhibition increases as the star’s surface field increases.

Extrapolating the dependence of equation (8) to larger values of R_A/R_* , we obtain, for example, for $R_A/R_* = 30$ an accretion rate $\dot{M}/\dot{M}_B \sim 2.67 \times 10^{-4}$ and a luminosity $L \sim 2.3 \times 10^{25}$ ergs s^{-1} , which is much smaller than that expected for the nonmagnetized star. IONSs with such a small luminosity are at present undetectable.

5. DISCUSSION AND CONCLUSIONS

The considered axisymmetric flows do not include the possibility of three-dimensional instabilities, which may increase the accretion rate in the equatorial plane (Arons & Lea 1976a, 1976b). The importance of these instabilities needs to be investigated with the three-dimensional MHD simulations.

Michel (1977b) proposed that accretion along the magnetic poles occurs through the formation of “drops” in the polar region when the density of the plasma becomes sufficient to push the magnetic field lines aside. This phenomenon is two-dimensional, so it is included in our axisymmetric simulations. However, we did not observe such a behavior. One of the reasons is that plasma does not accumulate above the magnetic poles in any significant quantities. Dense polar columns form, but the matter in the columns flows *steadily* to the surface of the star.

Note that we have chosen the Bondi accretion flow as an initial and boundary condition because this gives a steady flow in the nonmagnetic case. Also, the nonmagnetic Bondi flow has been well investigated analytically and numerically. We observed that a new regime of accretion forms around the magnetized star, so the Bondi flow represents a useful initial condition (see also T99). Test simulations at less than the Bondi accretion rate shown results similar to those presented here. However, the magnetosphere radius R_A is even larger than in the Bondi case, because the accretion rate \dot{M} is smaller. The accretion rate to the surface of the star is even smaller.

The results presented here are also applicable to the wind-fed X-ray pulsars. However, the angular momentum of incoming matter in the binary system may be larger in X-ray pulsars, and disk accretion is more probable than in the case of IONSs.

The main conclusions of this work are as follows:

1. For matter accreting spherically to a magnetized star with the Bondi accretion rate \dot{M}_B , an outward-propagating shock wave forms. Inside this shock wave a new stationary, subsonic accretion flow is established. Accretion to the surface of the star occurs along two columns along the magnetic axis of the star. Outside of the Alfvén radius the flow is approximately spherical, while inside this radius the flow is collimated by the star’s magnetic field. The flow is subsonic except at the throat, or critical point, of the flow near the surface of the star, where the flow becomes sonic.

2. Only a fraction of the Bondi flux \dot{M}_B accretes to the surface of the star, $\dot{M} = k\dot{M}_B$, where $k < 1$. The empirical dependences we find are $\dot{M}/\dot{M}_B \propto (R_*/R_A)^5$ for $R_A/R_* \sim 6-10$, where R_A is the Alfvén radius. In terms of the star’s magnetic moment μ , we find $\dot{M}/\dot{M}_B \propto \mu^{-3}$.

3. The accretion rate to the surface of the star decreases as the magnetic diffusivity of the plasma η_m decreases, $\dot{M} \propto (\eta_m)^{0.6}$.

4. Even if the residual magnetic field of IONSs is very small, we still have $R_A/R_* \gg 1$, so accretion to the surfaces of the stars is greatly reduced from the Bondi rate. The luminosities will be correspondingly reduced and may be undetectable with present instruments. The R_A/R_* values in our simulations correspond approximately to the case of neutron stars with very small surface magnetic fields, $B \sim 10^6$ G. Thus, our simulation results indicate a strong inhibition of accretion to even very weakly magnetized neutron stars. The inhibition increases as the star’s surface field increases.

This work was supported in part by NASA grant NAG 5-9047, NSF grant AST 99-86936, and the Russian program “Astronomy.” M. M. R. is grateful to an NSF POWRE grant for partial support. O. D. T. thanks INTAS grant 01-491. R. V. E. L. was partially supported by grant NAG

5-9735. The authors thank V. V. Savelyev for the original version of the MHD code, J. Stinchcombe for editing the manuscript, and the anonymous referee for valuable comments.

REFERENCES

- Arnett, W. D., Schramm, D. N., & Truran, J. W. 1989, *ApJ*, 339, L25
 Arons, J., & Lea, S. M. 1976a, *ApJ*, 207, 914
 ———. 1976b, *ApJ*, 210, 792
 Beloborodov, A. M., & Illarionov, A. F. 2001, *MNRAS*, 323, 167
 Bisnovatyi-Kogan, G. S., & Lovelace, R. V. E. 1997, *ApJ*, 486, L43
 ———. 2000, *ApJ*, 529, 978
 Blaes, O., & Madau, P. 1993, *ApJ*, 403, 690
 Blaes, O., Warren, O., & Madau, P. 1995, *ApJ*, 454, 370
 Bondi, H. 1952, *MNRAS*, 112, 195
 Bondi, H., & Hoyle, F. 1944, *MNRAS*, 104, 273
 Colpi, M., Turolla, R., Zane, S., & Treves, A. 1998, *ApJ*, 501, 252
 Cordes, J. M., & Chernoff, D. F. 1998, *ApJ*, 505, 315
 Davidson, K., & Ostriker, J. P. 1973, *ApJ*, 179, 585
 Davies, R. E., Fabian, A. C., & Pringle, J. E. 1979, *MNRAS*, 186, 779
 Davies, R. E., & Pringle, J. E. 1981, *MNRAS*, 196, 209
 Elsner, R. F., & Lamb, F. K. 1977, *ApJ*, 215, 897
 Igumenshchev, I. V., & Narayan, R. 2002, *ApJ*, 566, 137
 Ikhsanov, N. R. 2002, *A&A*, 381, L61
 Ikhsanov, N. R., & Pustil'nik, L. A. 1996, *A&A*, 312, 338
 Illarionov, A. F., & Sunyaev, R. A. 1975, *A&A*, 39, 185
 Kazhdan, Ya. M., & Lutskii, A. E. 1977, *Astrophysics*, 13, 301
 Kazhdan, Ya. M., & Murzina, M. 1994, *MNRAS*, 270, 351
 Koldoba, A. V., Lovelace, R. V. E., Ustyugova, G. V., & Romanova, M. M. 2002, *AJ*, 123, 2019
 Lipunov, V. M. 1992, *Astrophysics of Neutron Stars* (Berlin: Springer)
 Livio, M., Xu, C., & Frank, J. 1998, *ApJ*, 492, 298
 Lovelace, R. V. E., Romanova, M. M., & Bisnovatyi-Kogan, G. S. 1999, *ApJ*, 514, 368
 Madau, P., & Blaes, O. 1994, *ApJ*, 423, 748
 Michel, F. C. 1977a, *ApJ*, 213, 836
 ———. 1977b, *ApJ*, 214, 261
 ———. 1977c, *ApJ*, 216, 838
 Narayan, R., & Ostriker, J. P. 1990, *ApJ*, 352, 222
 Ostriker, J. P., McCray, R., Weaver, R., & Yahil, A. 1976, *ApJ*, 208, L61
 Ostriker, J. P., Rees, M. J., & Silk, J. 1970, *Astrophys. Lett.*, 6, 179
 Phinney, E. S., & Kulkarni, S. R. 1994, *ARA&A*, 32, 591
 Popov, S. B., Colpi, M., Treves, A., Turolla, R., Lipunov, V. M., & Prokhorov, M. E. 2000, *ApJ*, 530, 896
 Ruffert, M. 1994, *ApJ*, 427, 342
 Romanova, M. M., Toropina, O. D., Toropin, Yu. M., & Lovelace, R. V. E. 2003, *ApJ*, 588, 400
 Sakashita, S. 1974, *Ap&SS*, 26, 183
 Sakashita, S., & Yokosawa, M. 1974, *Ap&SS*, 31, 251
 Schvartsman, V. F. 1971, *Soviet Astron.—AJ*, 14, 662
 Toropin, Yu. M., Toropina, O. D., Savelyev, V. V., Romanova, M. M., Chechetkin, V. M., & Lovelace, R. V. E. 1999, *ApJ*, 517, 906 (T99)
 Toropina, O. D., Romanova, M. M., Toropin, Yu. M., & Lovelace, R. V. E. 2001, *ApJ*, 561, 964
 Treves, A., & Colpi, M. 1991, *A&A*, 241, 107
 Treves, A., Turolla, R., Zane, S., & Colpi, M. 2000, *PASP*, 112, 297
 Urpin, V. A., & Konenkov, D. 1997, *MNRAS*, 292, 167
 Urpin, V. A., & Muslimov, A. G. 1992, *MNRAS*, 256, 261
 Wang, Y.-M., & Robertson, J. A. 1985, *A&A*, 151, 361
 Zhukov, V. T., Zabrodin, A. V., & Feodoritova, O. B. 1993, *Comput. Maths. Math. Phys.*, 33(8), 1099